coatings

MDPI

Article

Pulsed Laser Deposited Biocompatible Lithium-Doped Hydroxyapatite Coatings with Antimicrobial Activity

Liviu Duta [1,*], Mariana Carmen Chifiriuc [2,3], Gianina Popescu-Pelin [1], Coralia Bleotu [4], Gratiela (Pircalabioru) Gradisteanu [3], Mihai Anastasescu [5], Alexandru Achim [6] and Andrei Popescu [6,*]

1 National Institute for Lasers, Plasma and Radiation Physics, 077125 Magurele, Romania; gianina.popescu@inflpr.ro
2 Department of Microbiology, Faculty of Biology, University of Bucharest, 060101 Bucharest, Romania; carmen.chifiriuc@gmail.com
3 Earth, Environmental and Life Sciences Division, Research Institute of the University of Bucharest (ICUB), 060101 Bucharest, Romania; gratiela87@gmail.com
4 "Stefan S. Nicolau" Institute of Virology, 030304 Bucharest, Romania; cbleotu@yahoo.com
5 "Ilie Murgulescu" Institute of Physical Chemistry, Romanian Academy, 060021 Bucharest, Romania; manastasescu_ro@yahoo.com
6 Center for Advanced Laser Technologies (CETAL), National Institute for Lasers, Plasma and Radiation Physics, 077125 Magurele, Romania; alexandru.achim@inflpr.ro
* Correspondence: liviu.duta@inflpr.ro (L.D.); andrei.popescu@inflpr.ro (A.P.)

Received: 5 December 2018; Accepted: 16 January 2019; Published: 17 January 2019

Abstract: Simple and lithium-doped biological-origin hydroxyapatite layers were synthesized by Pulsed Laser Deposition technique on medical grade Ti substrates. Cytotoxic effects of lithium addition and the biocompatibility of obtained coatings were assessed using three cell lines of human origin (new initiated dermal fibroblasts, immortalized keratinocytes HaCaT, and MG-63 osteosarcoma). Antimicrobial properties of obtained coatings were assessed on two strains (i.e., *Staphylococcus aureus* and *Candida albicans*), belonging to species representative for the etiology of medical devices biofilm-associated infections. Our findings suggest that synthesized lithium-doped coatings exhibited low cytotoxicity on human osteosarcoma and skin cells and therefore, an excellent biocompatibility, correlated with a long-lasting anti-staphylococcal and -fungal biofilm activity. Along with low fabrication costs generated by sustainable resources, these biological-derived materials demonstrate their promising potential for future prospective solutions—viable alternatives to commercially available biomimetic HA implants—for the fabrication of a new generation of implant coatings.

Keywords: lithium-doped hydroxyapatite coatings; renewable resources for implant coatings; pulsed laser deposition; biocompatibility; inhibition of microbial biofilms development

1. Introduction

Microbial biofilms development on medical devices and human tissues represents a serious public health problem at global level, leading to a high diversity of biofilm-associated infections, with increasing incidence, although yet underestimated and high rates of morbidity and mortality. The biofilm growth protects microbial cells from antimicrobials and host immune effectors, enabling pathogens to survive in limited conditions and also to disperse and colonize new niches. The biofilm-embedded microbial cells exhibit a high tolerance to conventional antimicrobial agents,

explaining the chronic and relapsing character of the produced infections [1–3]. The increasing incidence of biomaterial-associated infections is in close relationship with the continuously growing demand for implantable medical devices and other invasive diagnostic and therapeutic maneuvers. Therefore, controlling biofilm formation represents a mandatory feature during medical devices manufacturing and their use [4].

Biofilm development is a dynamic and complex process which occurs in several stages [1]. It starts with a reversible adhesion stage, followed by irreversible adhesion [5], maturation and, in the last stage, detachment. The first stages depend on the physico-chemical properties of the surface, conditioning the interactions with microbial structure involved in the adhesion process [6]. The main pathogens involved in the development of biofilm-associated infections include the Gram-positive bacteria, such as *Staphylococcus aureus* (*S. aureus*), and fungal strains, especially *Candida* spp. Reports from the National Institutes of Health demonstrate that around 80% of human infections are due to biofilms [7]. The biofilm-associated infections are characterized by moderate intensity symptoms, chronic evolution and high resistance to antibiotics [8]. Therefore, one main direction bridging materials science to biomedical research is the development of complex therapeutic strategies, including the association of multiple antimicrobial agents [9–11]. However, one should note that the association of multiple antibiotics might lead to high toxicity effects, correlated with a low efficiency on the cells embedded in biofilms [12]. Therefore, the development of preventive measures, based on the design of novel biomaterials, synthesized in the form of thin layers and used for the fabrication of medical devices which are more resistant to microbial colonization and biofilms development could represent a more effective approach [13,14].

Synthetic hydroxyapatite (HA) represents a well-known biocompatible material used as implantable ceramic due to its great chemical and structural resemblance to the inorganic part of human hard tissues [15,16]. Reports from dedicated literature have demonstrated that biological-derived HA (BHA) has some important advantages over synthetic HA. In this respect, to improve mechanical (anchorage to bone) and biological (osseointegration, resistance to microbial colonization) properties of medical implants, simple BHA materials [17] or BHA doped with specific reagents such as ZnO [18], SiO_2, MgO, Al_2O_3 and ZrO_2 [19], Ti [20], Li_2CO_3 and Li_3PO_4 [21], Li_2O [22], commercial inert glass [22,23], $CaMgSiO_6$ [24], MgF_2 or MgO [25], and CO_2 [26] have been used [27].

The present study is a first attempt in dedicated literature to fabricate, in a single-stage pulsed laser deposition process, BHA coatings to exhibit low cytotoxicity and good biocompatibility, corroborated with an active role in prevention of microbial colonization and biofilm development on prosthetic devices.

2. Materials and Methods

2.1. PLD Experimental Protocol

BHA powders were obtained from the femoral bones of freshly slaughtered cattle (received from a Turkish slaughter house, which uses the other animal parts for general consumption). Bones were delivered on ice to the laboratory and, before usage, they were submitted to a veterinary control. Concisely, both heads of femoral bones were cut off (because they contained too much soft tissue) and only femoral shafts were further processed. Bone marrows were extracted and all other soft tissue residues were removed from shafts. Then, femoral shafts were cut into slices, cleaned and washed with distilled water. Cleaned parts were deproteinized for 14 days in an alkali solution of 1% sodium hypochlorite. After washing and drying, bone pieces were calcinated at 850 °C for 4 h in air, in order to completely eliminate organic components of bone. We emphasize that as-prepared BHA powders are biologically safe due to the high temperature fabrication route, which not only favors the crystallization of the material, but also totally prevents any risk of diseases transmission, as no pathogen can survive to such extreme conditions [20–22,25]. Resulting calcined bone specimens were first crushed with a mortar and pestle and then ball-milled (for 4 h) to fine powders (i.e., with particles

of submicron size). The color of the resulting powders was milky-white. One should note that the experimental procedure for the fabrication of BHA powders was conducted in accordance with the European Regulation 722/2012 [28] and ISO 22442:2015 standard [29]. Batches of BHA powders were admixed with 1 wt.% of Li_2CO_3 or Li_3PO_4 (Sigma-Aldrich GmbH, St. Louis, MO, USA). Sample codes are introduced in Table 1 and will be further used in the text.

Table 1. Sample codes and description.

Sample Code	Sample Description
Ti	Bare Ti control
Si	Simple Si control
Li-0	Simple BHA film deposited on Ti
Li-C	BHA:Li_2CO_3 film deposited on Ti
Li-P	BHA:Li_3PO_4 film deposited on Ti

PLD experiments were carried out inside a stainless-steel deposition chamber. A KrF * excimer laser source COMPex Pro205 (Coherent, Göttingen, Germany) (λ = 248 nm, $\tau_{FWHM} \leq$ 25 ns, υ = 10 Hz) was used for target irradiation.

The laser beam was oriented at 45° in respect with the target surface. The laser fluence incident onto the target surface was set at ~4 J/cm^2 (with a corresponding pulse energy of ~360 mJ).

Before deposition, targets were "cleaned" by short multipulse laser ablation with 1000 pulses. During deposition, the target was continuously rotated with 0.4 Hz and translated along two orthogonal axes to avoid piercing and allow for the growth of uniform films.

The ablated material was collected onto medical-grade titanium (Ti) disks (~0.6 × 0.6 cm^2 and 0.1 cm thickness), that were placed parallel to the target at a separation distance of 5 cm.

All experiments were performed in a 50 Pa water vapor atmosphere. During experiments, substrates were heated and maintained at a constant temperature of 500 °C using a PID-EXCEL temperature controller (Excel Instruments, Gujarat, India). A heating rate of 25 °C/min and a cooling ramp of 10 °C/min have been used. For the deposition of each structure, 15,000 subsequent laser pulses were applied.

So as to improve the crystalline status of synthesized films, all samples have been subjected to a 6 h post-deposition thermal treatment in air (in water vapors), at 600 °C.

2.2. Characterization of Synthesized Structures

2.2.1. Atomic Force Microscopy

The surface topography of synthesized structures was examined in high resolution Atomic Force Microscopy (AFM) (Park Systems, Suwon, Korea), performed in the non-contact mode on a XE-100 apparatus from Park Systems. Sharp tips (PPP-NCHR type from Nanosensors^{TM}, Neuchâtel, Switzerland), having 125 μm in length, 30 μm width and radius of curvature of less than 8 nm, were used at surface scanning over areas of 0.5 × 0.5 μm^2. The spring constant was of ~42 N/m and the resonance frequency of ~330 kHz, respectively. All AFM measurements were performed at room temperature.

AFM images were processed using Image Processing Program, XEI–v.1.8.0, developed by Park Systems (Suwon, Korea). The horizontal line by line flattening was used as planarization method for displaying purposes and for subsequent statistical data analysis, including the calculation of the roughness. To have a better view of the surface morphology, 2D-AFM images are displayed in the classical view mode (one color used also for the z-scale bar), while 3D-AFM images are shown as topographic maps in the so-called "enhanced color" view mode (using the change of a pixel color relative to its neighbors).

The textural (amplitude) parameters, namely average roughness (R_a), surface skewness (R_{sk}) and surface kurtosis (R_{ku}) were determined giving information about the roughness and the degree of

skewness and kurtosis of investigated surfaces. R_a is the area between the roughness and its mean in contrast with the root-mean-squared roughness, which is the standard deviation of the height value in the selected region. In statistics, R_{sk} is a measure of the asymmetry of the probability distribution of a real-valued random variable about its mean. In the present case, R_{sk} describes the asymmetry of the height distribution (frequency vs. height histogram). R_{ku} measures the randomness of profile heights and of the "sharpness" of the height distribution, and has a value of 3 in the case of a perfectly random surface [30]. Kurtosis is not related to the geometry of the distribution, but to the shape of it. Kurtosis is a measure of whether data are heavy-tailed or light-tailed, relative to a normal distribution (R_{ku} = 3). Thus, data sets with high kurtosis, $R_{ku} > 3$ (sharper height distributions–so called "lepto kurtosis") tend to have heavy tails, or outliers. Data sets with low kurtosis, $R_{ku} < 3$ (flattened height distribution–so called "platy kurtosis"), tend to have light tails, or lack of outliers.

2.2.2. In Vitro Biological Tests

The potential use of synthesized coatings in the biomedical field was appraised by both safety (cytotoxicity and influence on the cellular cycle of three different human cell lines) and anti-biofilm tests (performed on bacterial and fungal strains).

Biocompatibility Assays

(i) Cytotoxicity Assays

The cytotoxicity of obtained coatings was investigated using three different cell lines, i.e., MG-63 osteosarcoma ECACC 86051601, new initiated dermal fibroblasts (FBD) and immortalized keratinocytes HaCaT [31].

The cytotoxicity of samples was investigated after microscopic examination of the unstained monolayers developed on their surface. Changes of the general morphology and monolayer confluence were assessed. The cytotoxicity level of the tested samples was classified in accordance to the ISO standard recommendations [32].

The UV-sterilized samples were placed in duplicate in 24-well plates exposing the coated face. A total of 1×10^5 cells in Dulbecco's Modified Eagle Medium:F12 supplemented with 10% fetal bovine serum were added. Plates were maintained for 24 h at 37 °C and 5% CO_2 atmosphere. After 24 h, samples have been observed with an inverted microscope and photographed in contrast phase with a Zeiss Observer D1 microscope (Zeiss, Oberkochen, Germany). Due to the fact that BHA samples were opaque, the examination and images of cellular monolayers were taken in the vicinity of tested materials. Then, one of the duplicate samples was extracted from the well, fixed in ethanol 70%, stained for 5 min with propidium iodide (PI) (chemical name 3,8-Diamino-5-(3-(diethyl(methyl)ammonio)propyl)-6-phenylphenanthridin-5-ium iodide) 50 µg/mL, and visualized in red channel, using a fluorescence Leica DFC450C microscope (Leica, Allendale, NJ, USA).

(ii) Cellular Cycle Assay

For the investigation of the cellular cycle, samples (treated as mentioned in the previous section) were harvested with trypsin, fixed in 70% cold ethanol over night at −20 °C, and then washed with phosphate-buffered saline (pH 7.5), treated with 100 µg/mL RNase A for 15 min and stained with 10 µg/mL PI for 1 h at 37 °C. After PI staining, the events (number of cells passing through the laser) acquisition was performed with an Epics Beckman Coulter flow cytometer (Beckman Coulter Inc., Indianapolis, IN, USA). The obtained data was analyzed with the FlowJo software 7.6.4 and expressed as fractions of cells found in different cell cycle phases [33].

Antimicrobial Assays

Two microbial strains traceable to American Type Culture Collection (ATTC), belonging to two of the most important species known to be involved in the etiology of medical devices biofilm-associated infections, respectively *S. aureus* and *Candida albicans* (*C. albicans*), were used in the experiments. Fresh cultures were obtained from glycerol stocks of *S. aureus* ATTC 6538 and *C. albicans* ATTC 26790 strains on non-selective solid media. Samples were sterilized by exposure to UV irradiation in a laminar flow chamber for 30 min on each side, placed in duplicate in six-well plates (Nunc) in 2 mL of Luria Broth (LB) nutrient medium and then inoculated with 500 µL of standardized microbial suspensions of 0.5 McFarland density corresponding to ~10^5–10^6 Colony Forming Units (CFU)/mL. After incubation at 37 °C, for different time periods (1, 6, 12, 24, 48 and 72 h, respectively), colonized samples were gently washed with distilled water to remove unattached microbial cells and then immersed in 1 mL sterile saline buffer in Eppendorf tubes, sonicated for 15 s, and then vortexed for 15 s at 3000 rotations/min. Suspensions resulted from the detached biofilms were then ten-fold diluted and 10 µL of each serial dilution were plated in triplicate on tryptic soy agar. After 24 h of incubation at 37 °C, colonies were counted and the number of CFU/mL was determined.

The surface characterization of inoculated surfaces was carried out using Scanning Electron Microscopy (SEM) with a FEI Inspect S50 apparatus (FEI, Hillsboro, OR, USA). Prior to this investigation, samples were washed three times in PBS and then fixed in ethanol, for 5 min, at RT.

3. Results

3.1. AFM Analysis

Typical bidimensional (2D) and tridimensional (3D) topographic images collected at a scanning area of (0.5 × 0.5) µm^2 are presented in Figure 1. The 3D AFM images, which are topographic maps of scanned areas, are presented in the Enhanced Color™ view mode (Park Systems) in order to better emphasize the morphological surface peculiarities. In 3D-AFM micrographs, dark color (blue) delineates surface "valleys", whilst the light color (orange) corresponds to the salient features ("hills"). The 2D AFM images are presented in the "classical" view mode, with one color gradient (brown in this case) for the z-scale depth. The first row presents the morphological features of the bare substrate (Si), which are located in a z-scale depth (Δz) of less than 1 nm (typical ~0.7 nm), which leads to a very low R_a value of only 0.1 nm (which is representative for a clean Si wafer), as seen in Table 2. The R_{sk} parameter, describing the asymmetry of the height distribution histogram, has a small value in this case, of 0.9, which is corresponding to a flat surface with random (small) protuberances. The R_{ku} parameter, which represents a measure of the randomness of the profile heights and of the "sharpness" of the surface height distribution, has a value of ~3, which is characteristic for a near perfect random surface (Gaussian distribution) [30].

Li-0 films (Figure 1–second row) exhibit protruding (R_{sk} ~0.46) large particles, randomly distributed (R_{ku} ~3.11), having tens of nm in diameter (~35–50 nm), individually displayed or with a tendency to merge. In this case, the average roughness increases to a value of ~5.9 nm, which is higher than the one registered for the bare substrate.

In the case of Li-C structures (Figure 1–third row), the addition of lithium leads to the formation of much larger particles, almost double as compared to Li-0 films and, accordingly, with a double roughness value (10.3 nm). Though, particles are not much more protruding in z direction, as the R_{sk} parameter is ~0.56, and relatively uniform distributed as the kurtosis parameter being just a bit higher (R_{ku} ~3.49) than in the second case.

Finally, in the case of Li-P structures (Figure 1–last row), the addition of lithium leads to a morphology similar to the one of Li-0 films, but with particles slightly smaller (diameters ~25 nm) and better separated (the fusing tendency being lower). Therefore, it exhibits the highest value for R_{ku} parameter in this series (5.58), pointing to a sharp height distribution [34], but with a lower skewness factor (0.17) as compared with Li-0 (0.46) and Li-C (0.56), which means that particles are less

protuberant for Li-P structures. This leads to an average roughness value (4.32 nm) very close to the one characteristic for Li-0 films (5.9 nm).

Overall, based on the results, one should emphasize that the obtained lithium-based structures could be described as homogeneous and uniform, with a morphology that depends on the preparation route and with (average) roughness values in the nanometric range (R_a ~5–10 nm).

The inferred values of the amplitude parameters, which were discussed above, are summarized in Table 2.

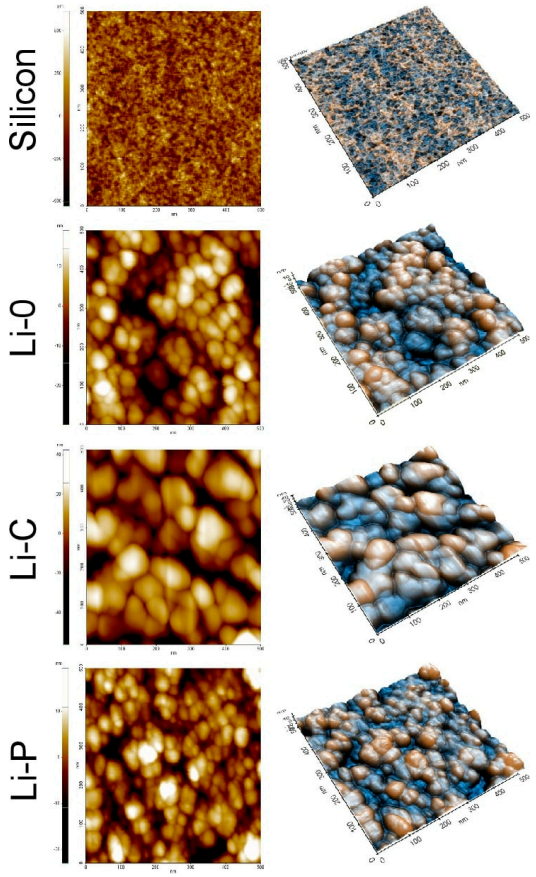

Figure 1. The 2D (classical view mode—left column) and 3D (enhanced color view mode—right column) AFM images of Li-0, Li-C and Li-P structures synthesized at 600 °C on Si(100) wafers.

Table 2. Surface amplitude parameters (R_a, R_{sk} and R_{ku}) for a (0.5 × 0.5 μm^2) scanned surface area of control (Si) and Li-0, Li-C and Li-P structures.

Sample Code	Amplitude Parameter	Scanning Area (0.5 × 0.5 μm^2)
Si	R_a (nm)	0.10
	R_{sk}	0.09
	R_{ku}	3.03
Li-0	R_a (nm)	5.86
	R_{sk}	0.46
	R_{ku}	3.11
Li-C	R_a (nm)	10.26
	R_{sk}	0.56
	R_{ku}	3.49
Li-P	R_a (nm)	4.32
	R_{sk}	0.17
	R_{ku}	5.58

3.2. Biocompatibility Assays

3.2.1. Cytotoxicity Test

In the current study, the cytotoxicity of obtained coatings was assessed using three cellular lines of human origin, selected for covering their diverse potential applications in the development of medical devices. Thus, MG-63 osteosarcoma cells exhibit common features with human osteoblast precursors or poorly differentiated osteoblasts, producing type I collagen with no or reduced osteocalcin and alkaline phosphatase basal level, making them appropriate for assessing the biocompatibility of biomaterials designed for orthopedic applications [35,36]. The other two cell lines were represented by human skin new initiated dermal fibroblasts and human skin immortalized keratinocytes, considering that many implanted medical devices or next generation wound dressings are coming for short time into contact with the skin.

Concerning the cytotoxicity of synthesized materials, contrast phase microscopy images (Figures 2–4) have shown that cells developed on plastic well, at the limit with the tested disc surface, are unaffected and preserved an unmodified morphology. This suggests that BHA materials do not release toxic substances in the environment, as secondary product. New initiated dermal fibroblasts exhibited a spindle-shaped morphology (Figure 2), the morphological appearance of keratinocytes showed polygonal cells (Figure 3), whilst MG-63 monolayers were composed of elongated and fusiform cells (Figure 4).

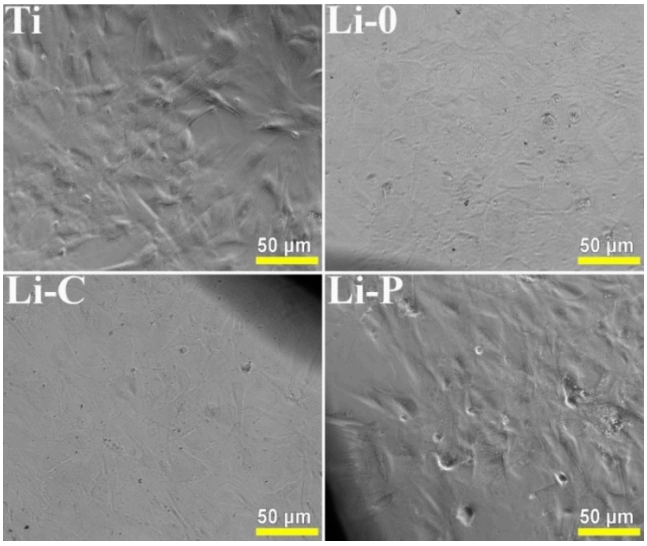

Figure 2. Contrast phase inverted microscopy images of the new initiated dermal fibroblasts monolayer grown in the presence of Ti and simple and doped biological-derived HA coatings (Magnification ×200).

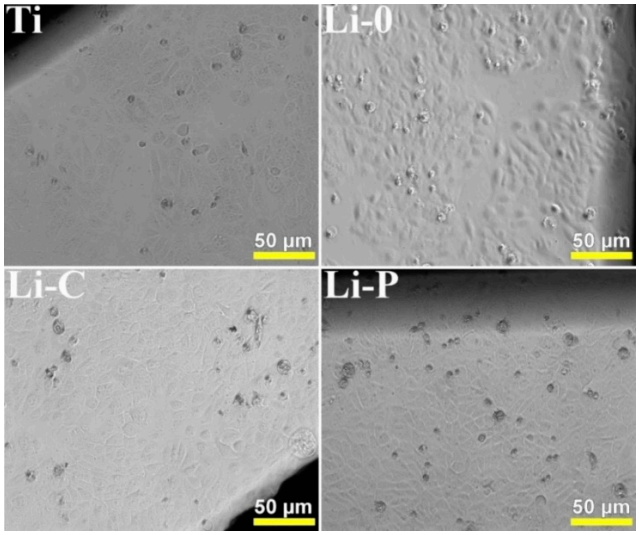

Figure 3. Contrast phase inverted microscopy images of the immortalized keratinocytes HaCaT monolayer grown in the presence of Ti and simple and doped biological-derived HA coatings (Magnification ×200).

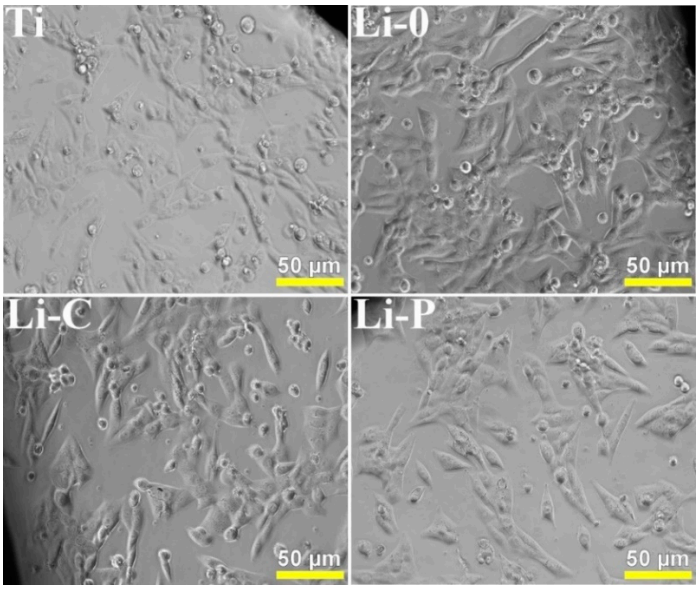

Figure 4. Contrast phase inverted microscopy images of the MG-63 osteosarcoma cells monolayer grown in the presence of Ti and simple and doped biological-derived HA coatings (Magnification ×200).

On the other hand, the fluorescence microscopy images (Figures 5–7) have revealed that the number of adhered cells on the bare Ti was similar between all synthesized layers and depends on type of cell line. This observation suggests that deposited layers are not cytotoxic against human skin or bone cells and allow for an unhindered cell development. According to the ISO standard specifications [32], the cytotoxic effect of synthesized layers can be classified as absent, supporting the potential of fabricated materials to be used as coatings for different biomedical surfaces, such as orthopedic devices, dental materials, or catheters.

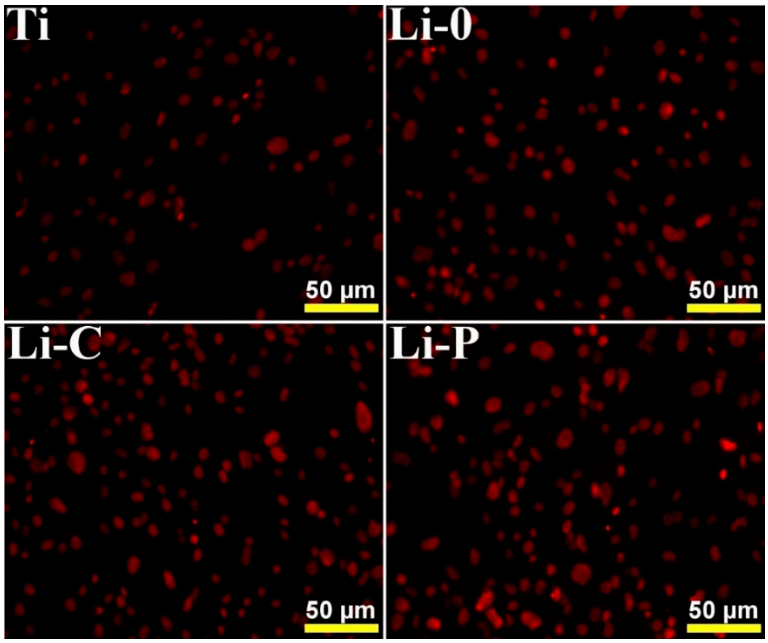

Figure 5. Fluorescence microscopy images of new initiated dermal fibroblasts grown for 24 h on the surface of Ti and simple and doped biological-derived HA coatings (Magnification ×200).

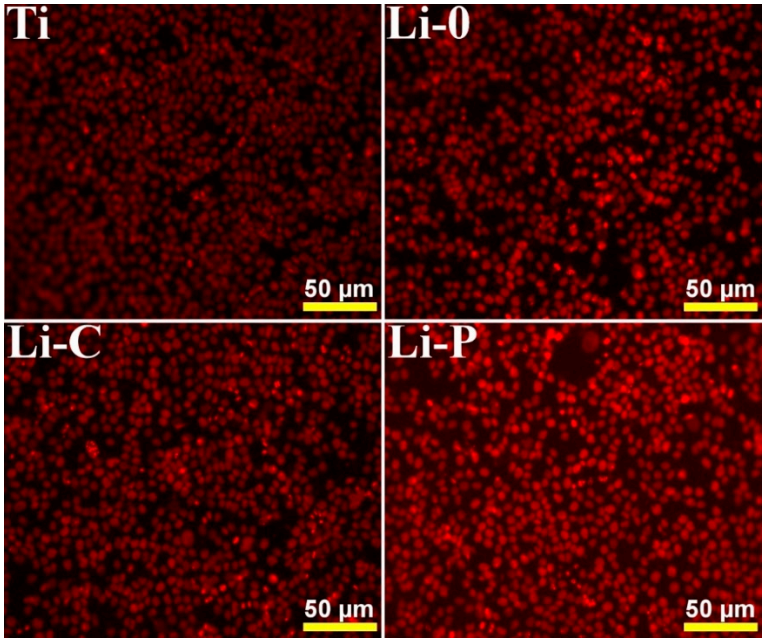

Figure 6. Fluorescence microscopy images of immortalized keratinocytes HaCaT grown for 24 h on the surface of Ti and simple and doped biological-derived HA coatings (Magnification ×200).

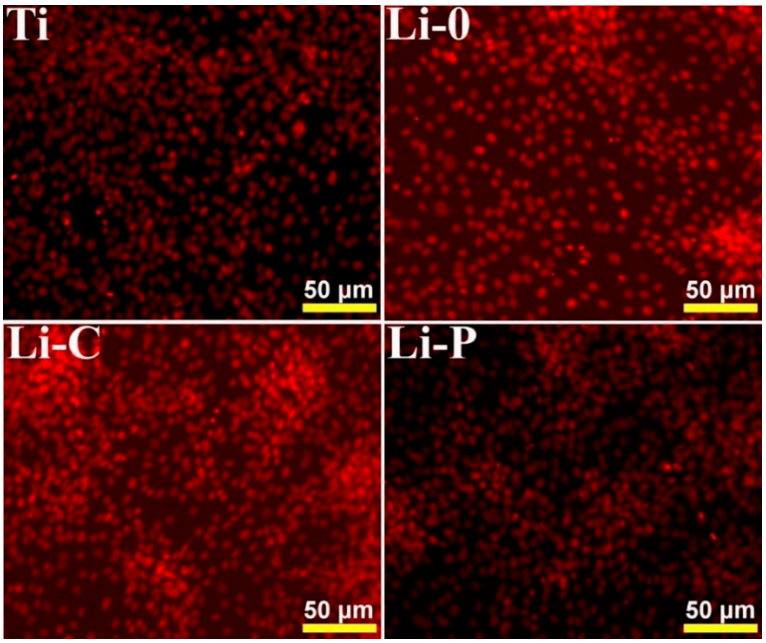

Figure 7. Fluorescence microscopy images of MG-63 osteosarcoma cells grown for 24 h on the surface of Ti and simple and doped biological-derived HA coatings (Magnification ×200).

3.2.2. Cellular Cycle Assay

The cell cycle analysis by flow cytometry revealed that the obtained coatings did not influence the cellular cycle progression of the three type of cells (i.e., new initiated dermal fibroblasts, immortalized keratinocytes and MG-63 osteosarcoma cells) (Figures 8–10), confirming that synthesized layers do not interfere with the typical development of normal and tumoral cells.

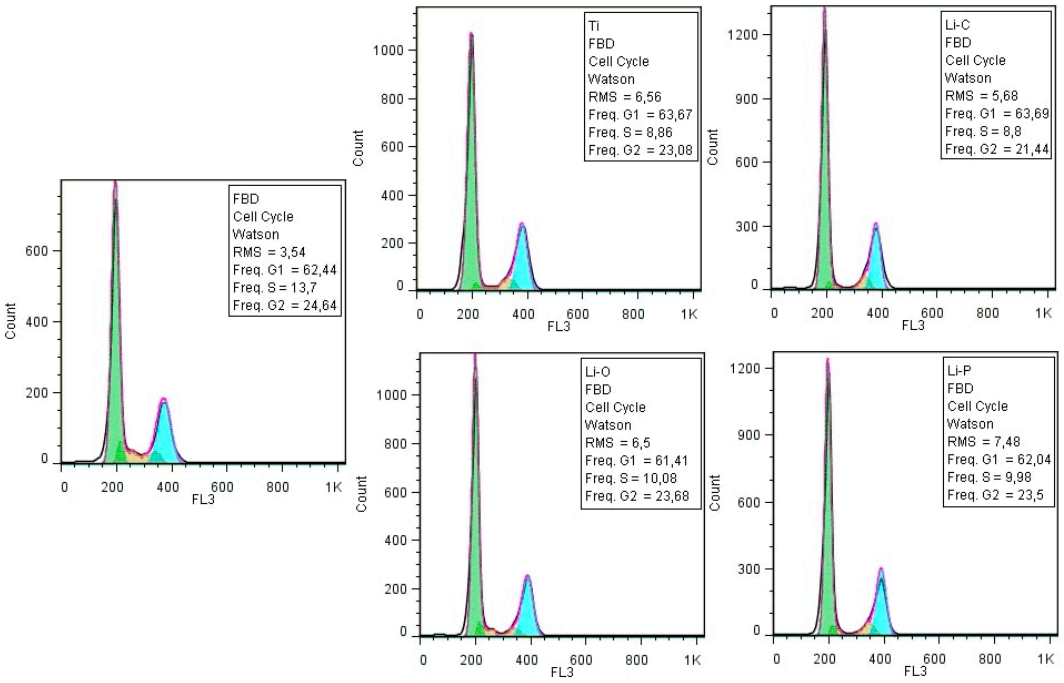

Figure 8. Flow cytometry diagrams of cells cycle analysis of new initiated dermal fibroblasts grown on the tested materials.

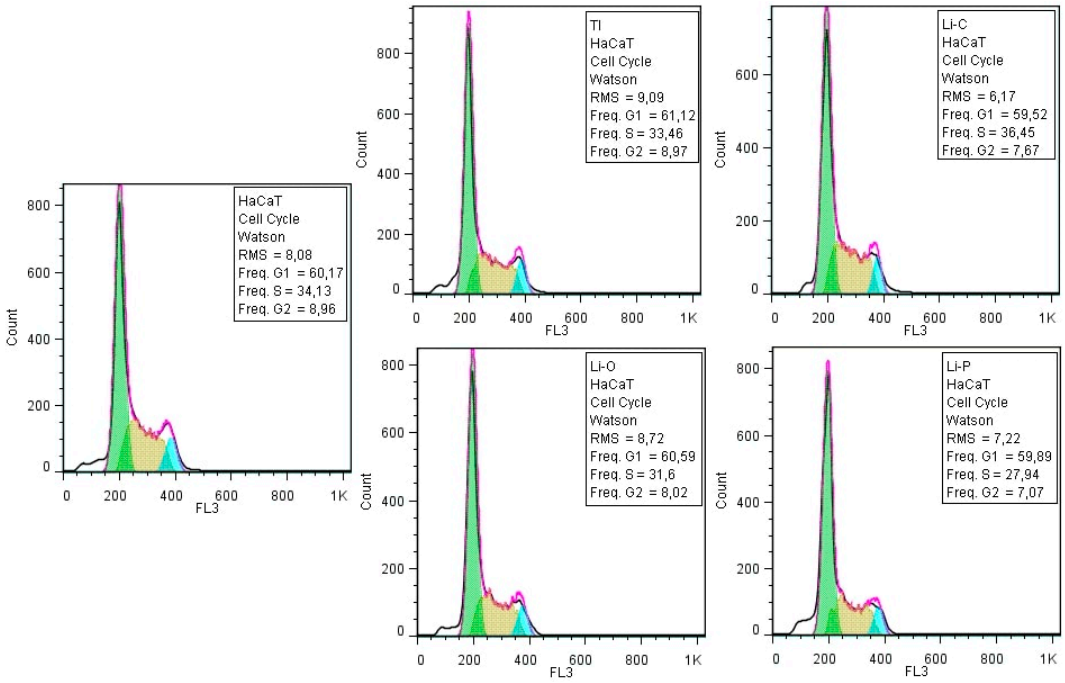

Figure 9. Flow cytometry diagrams of cells cycle analysis of immortalized keratinocytes grown on the tested materials.

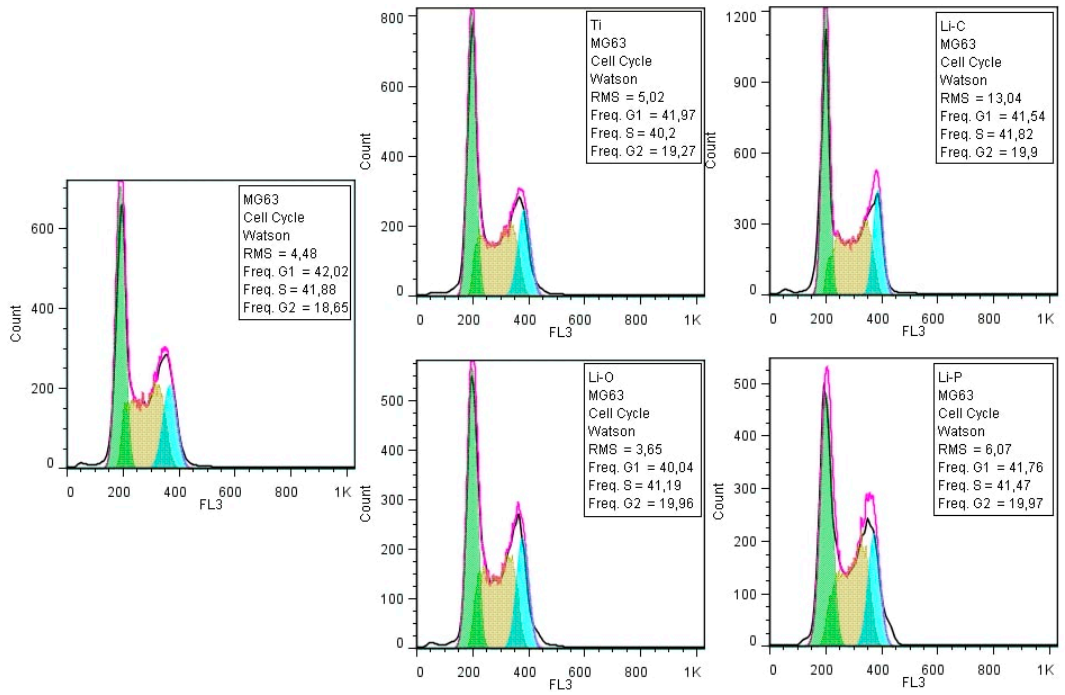

Figure 10. Flow cytometry diagrams of cells cycle analysis of MG-63 osteosarcoma cells grown on the tested materials.

3.3. Anti-Biofilm Activity

3.3.1. Anti-Staphylococcal Biofilm Activity of Obtained Coatings

Compared with Ti, after 24 h of incubation, all tested coatings exhibited a significant inhibitory activity against *S. aureus* biofilm growth, showing a significant increase starting with 48 h of incubation and persisting with high intensity, after 72 h of incubation. This behavior is suggested by the drastic decrease of the number of CFU/mL by 2 to 4 logs at these last two-time intervals (Figure 11b). The

absence of a visible inhibition of the microbial growth in the 1–2 h (Figure 11a) interval reveals that the anti-biofilm effect is possibly due to the slow release of some bioactive components from the synthesized coatings, with potential antimicrobial activity (e.g., oligoelements).

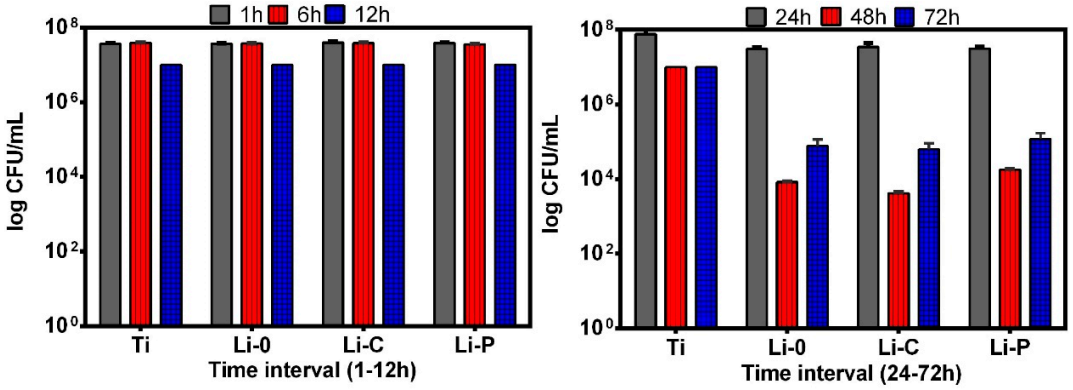

(**a**) (**b**)

Figure 11. Graphic representation of the logarithmic values of *S. aureus* biofilm cells developed on the surface of Ti and simple and doped biological-derived HA coatings: (**a**) 1–12 h and (**b**) 24–72 h.

Regarding comparative efficiency of the tested materials, one can observe that Li-C coatings exhibited a slightly increased antimicrobial activity against *S. aureus* biofilm after 48 h of incubation, as compared to Li-0 and Li-P ones (Figure 11b).

The SEM images of *S. aureus* biofilm developed on the surface of Ti and simple and doped BHA structures are presented comparatively in Figure 12, at a magnification of 10,000×. For comparison reasons only non-inoculated simple and lithium-doped surfaces are presented by the authors of [21]. Although *S. aureus* adhered to all tested samples, it must be noticed that the density of *S. aureus* cells was significantly more reduced on Li-C > Li-P > Li-0 surfaces as compared to Ti ones, which is in good agreement with the quantitative results presented in Figure 11. SEM images of *S. aureus* biofilms are in concordance with others reported in the literature [1,37,38].

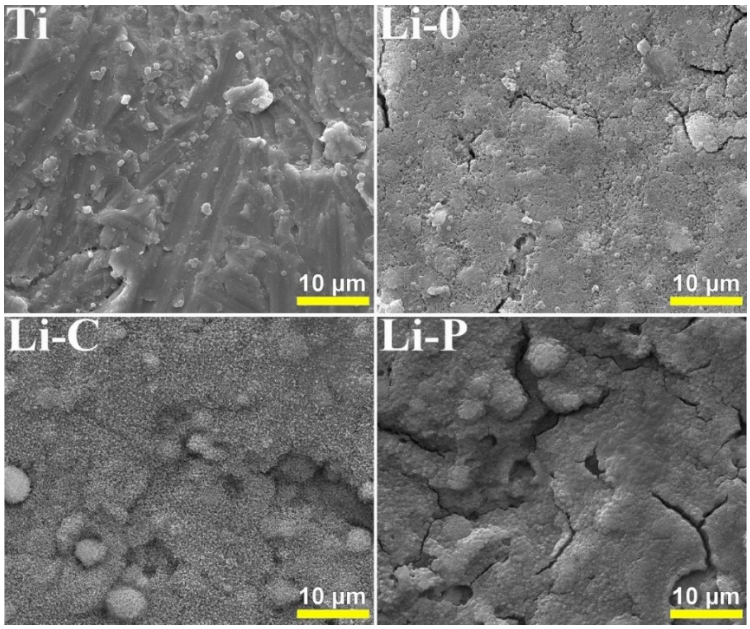

Figure 12. SEM images corresponding to *S. aureus* biofilm after 72 h of development on the surfaces of Ti and simple and doped biological-derived HA coatings.

3.3.2. Anti-Fungal Biofilm Activity of Obtained Coatings

In the case of *C. albicans* strain, a strong anti-biofilm effect was recorded for all tested coatings as compared to Ti, earlier than in the case of *S. aureus* biofilm, i.e., after 12 h of incubation (Figure 13a), followed by a recrudescence of microbial growth at 24 h and a drastic decrease of the biofilm-embedded cells at 48 and 72 h, respectively (Figure 13b). Moreover, Li-C and Li-P coatings proved a slightly better efficiency (as compared to Li-0 samples) against *C. albicans* biofilms incubated for 48 h, whilst Li-0 and Li-P showed the same antimicrobial efficiency at 72 h of incubation (Figure 13b).

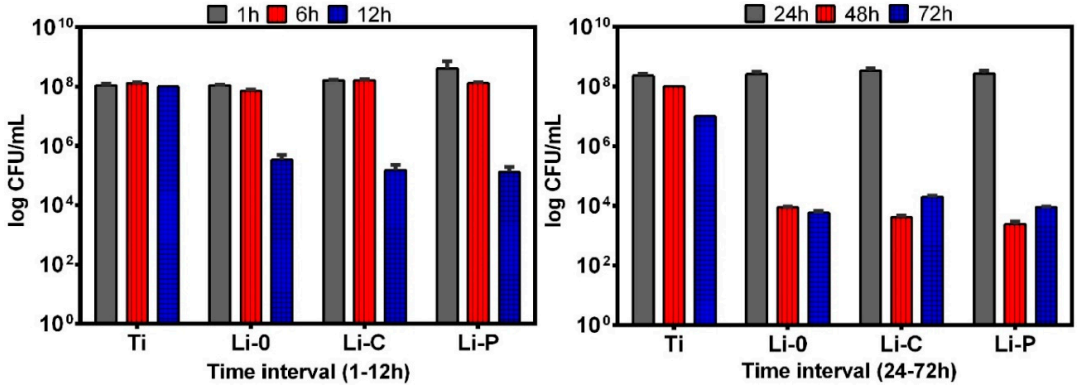

(**a**) (**b**)

Figure 13. Graphic representation of the logarithmic values of *C. albicans* biofilm cells developed on the surface of Ti and simple and doped biological-derived HA coatings: (**a**) 1–12 h and (**b**) 24–72 h.

The efficiency of the anti-fungal biofilm activity of simple and doped coatings decreased in the order Li-C, Li-P, Li-0, after an incubation time of three days (Figure 13).

Similar to the case of *S. aureus* strain, no visible inhibition of microbial development was obtained in the range of 1–6 h (Figure 13a), most probably due to the slow release from the synthesized films of the active elements responsible for the antimicrobial effect.

Following adherence to abiotic substrates (i.e., catheters and other medical devices), *C. albicans* develops into a three-dimensional community containing round-budding yeast cells, oval pseudo-hyphal cells and elongated hyphal cells embedded in an extracellular polysaccharides' matrix [39]. *C. albicans* biofilm development follows a sequential dynamic over a 24–48 h period, starting with initial adhesion of single fungal yeast cells, continuing with a cellular proliferation and colonization of the surface and the switching to filamentous hyphal forms, a hallmark of the initiation of biofilm formation, followed by maturation, through the accumulation of the protecting extracellular polysaccharide matrix. Dispersion of biofilm-associated cells from the mature biofilm can initiate formation of new biofilms or disseminate into host tissues, therefore being associated with candidemia and invasive fungal infections [40].

SEM images of *C. albicans* biofilm developed on the surface of Ti and simple and doped BHA structures are presented comparatively in Figure 14 at a magnification of 10,000×. In the case of bare Ti, one can observe many ovoidal or round-shaped cells which have the tendency to form micro-colonies, as well as the existence of filamentous, hyphal forms. Ti samples were completely covered by a continuous layer of cells, which is in good correlation with the quantitative results presented in Figure 13. This observation might be indicative not only for cell-surface type interactions, but also for stronger cell-cell type ones.

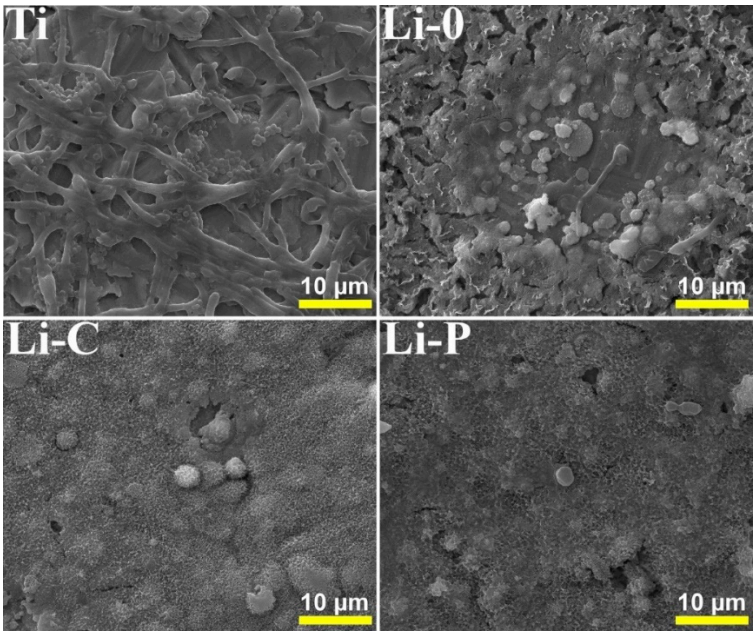

Figure 14. SEM images corresponding to *C. albicans* biofilm after 72 h of development on the surfaces of Ti and simple and doped biological-derived HA coatings.

In exchange, in case of coated surfaces, particularly Li-C and Li-P ones, the number of yeast cells is drastically decreased, they adhere exclusively in isolated, unicellular form, the filaments being completely absent.

The microscopy results demonstrate that the synthesized coatings inhibit the initiation of fungal biofilm development. SEM images of *C. albicans* are in concordance with others reported in literature [1,41].

We note that results of anti-biofilm quantitative assays, which revealed a slightly superior anti-biofilm effect of Li-C and Li-P structures as compared to control Ti and Li-0 ones, are in good agreement with aspects recorded in SEM examination (Figures 12 and 14). Presented SEM images were considered representative for the entire surface of samples and were selected after examining 8–10 different microscopic fields.

4. Discussion

4.1. Biocompatibility

Lithium is considered as a trace metal in organisms and is used for the treatment of bipolar affective disorder [42] and refractory depression [43]. The safe administration of lithium for osteoporosis was reported more than two decades ago [44,45]. When used in the low bone mass and osteoporosis-mice models, lithium was indicated to enhance osteogenesis [46]. Also, in the case of lumbar spine, femoral neck and proximal femur, the corresponding bone mineral density values were reported to be higher than controls [45,47]. Despite its proven efficacy and safety [48], there are cases when lithium administration could be toxic and determine side effects, such as thirst and excessive urination, nausea, diarrhea, tremor, weight gain, sexual dysfunction, dermatological effects, as well as long-term effects on the thyroid gland, kidneys and parathyroid glands [49]. However, recent studies challenge this negative perception of lithium administration, by showing strong evidence that intoxication in patients receiving lithium treatments is rare, it occurs only when the concentration is higher than 1.5 mmol/L, and its main adverse effects can be properly monitored and managed [50–52].

Even though its excellent biocompatibility was proven, the poor mechanical properties of HA limit its applications in implantology to non-load-bearing implants. It has been shown that ion doping represents a good method applied to improve performances of bio-ceramics related to biodegradability,

biocompatibility, strength and toughness. Therefore, when lithium is substituted into the HA structure, it plays an important role because it could induce a decrease in HA solubility [53,54], without affecting its biocompatibility [55,56], and an improvement of biomechanical properties, without altering the HA structure. The reason for the increase of strength of lithium doped HA may be due to the fact that metal ions could decrease the porosity of samples which can result in a more compact and hard structure [57]. Also, one notes that, as a substituted trace element, lithium can positively influence the viability [58], proliferation rates and alkaline phosphatase activity of cells [59,60]. Wang et al. [57] reported that when used in a proper low dose (0.5% and 1%), lithium ions can substitute calcium ones in a HA structure, in order to obtain a biomaterial (LiHA scaffold) characterized by high strength, a higher osteoblast-mediated degradation rate and a superior ability to promote cell proliferation as compared to simple HA and controls. On one hand, the lithium incorporation into HA can change the surface topography of original HA material and make LiHA scaffold possess a more compact bulk, which finally can result in a higher adherence and enhanced growth of osteoblasts [61]. On the other hand, the Li^+ released from LiHA scaffolds could enhance the activity of osteoblasts, a phenomenon also reported by Tang et al. [62]. In another study, Oh et al. [63] assessed the influence of lithium fluoride (LiF) on in vitro biocompatibility and bioactivity of calcium aluminate-polymethylmethacrylate composite cements. The results indicated that there was no cytotoxicity related to LiF and the addition of 1 wt.% LiF enabled composite cements to form HA on their surface within 15 days of soaking in SBF solutions. One can therefore conclude that these enhanced characteristics strengthen the safe use of lithium and could advance lithium-containing structures as promising materials for the fabrication of bone tissue engineering scaffolds.

The literature data on the cytotoxic ions release rates for lithium-substituted HA materials is rather scarce and reported cytotoxic levels are sometimes contradictory due to the fact that release rates are strongly depending on crystallinity or particle morphology and size of the investigated material [42]. In a current study, Miguez-Pacheco et al. [64] reported on lithium-containing bioactive glasses, with Li_2O substituting Na_2O in different amounts. The conclusion of their study, in terms of lithium ion release, was that formulations with 2.5 wt.% and 5 wt.% Li_2O content proved to be within the therapeutic range.

In vitro cytotoxicity assays of newly developed materials should precede in vivo tests, since the results are more reproducible and allow for the evaluation of cellular and molecular responses triggered by an investigated material [65].

We stress upon that results obtained on human skin new initiated dermal fibroblasts and human skin immortalized keratinocytes could be informative for the potential of the tested materials to be used in oral applications, for example in facial reconstruction, dental implants or periodontal pockets filling. A fully differentiated human gingiva equivalent was constructed entirely from keratinocytes and fibroblasts, being considered a valuable surrogate of animal models for testing new therapeutics [66]. Moreover, one could therefore predict the potential orthopedic implant-related adverse effects, related to the occurrence of hypersensitivity reactions to the implant material components. This evaluation is presently recommended for patients with a clear self-reported history of metal reactions and is done by patch testing before device implant [67].

4.2. Possible Mechanisms Explaining the Antimicrobial Activity of Synthesized Structures

We stress that infection still remains a major impediment to the long-term use of many implanted devices. Even though microbial adhesion to biomaterial surfaces represents an essential step in the pathogenesis of these infections, molecular and physical interactions that govern this adhesion have not been yet fully understood. Both specific and non-specific interactions may play an important role in the ability of cells to attach to (or to resist detachment from) the biomaterial surface [68]. In the biomedical field, a great number of implant failures is due to the formation of microbes at the implanted site. Microbes, which are able to cause a wide variety of infections in humans by spreading through common places like bathroom tiles, doorknobs, or packing materials, can be controlled by coating implants

with materials with antimicrobial properties. Antimicrobial implantable materials must locally kill microbes or slow down their growth, without being toxic to host tissue cells. Therefore, if an implant material will possess such characteristics, then the problem of failure will be drastically reduced.

Besides the utility of lithium in the treatment of mood disorders, different studies reported that as well as other antidepressants, it could exhibit an immunostimulant role and antimicrobial activity, as it opposes eicosanoids suppressive action upon the immune system [69]. Recent studies have shown that lithium could limit neurodegeneration and ameliorate symptoms of the trimethyltin poisoning in rodents, by inducing pro-survival and anti-inflammatory effects [70]. Moreover, in concentrations of up to 10 mol.%, lithium could enhance the antibacterial activity of bioactive glass against resistant bacteria, such as methicillin-resistant *S. aureus*. The 58S bioactive glass with 5 mol.% Li_2O substitution for CaO was considered a promising biomaterial in bone repair/regeneration therapies, showing an enhanced biocompatibility and alkaline phosphatase activity, with a negligible loss in the bioactivity compared to the 58S bioglass [71].

The adhesion ability of *S. aureus* to extracellular matrix components and plasma proteins from the pellicle formed on the surface of implanted biomaterials represents one main concern for infections associated to implanted medical devices. *C. albicans* is considered one of the major etiological agents of hospital-acquired infections, being also frequently associated with contamination of indwelling medical devices [72]. The phenotypic plasticity is a unique feature of many fungal species, including *C. albicans*, which is an extremely versatile, dimorphic yeast that can survive as a commensal in various environments, one of the adapting mechanisms being the switching from the yeast to filamentous forms [73]. *S. aureus* and *C. albicans* can be also found in multispecies biofilms, mutually potentiating their tolerance to antibiotics and disinfectants [74]. The mechanism of indirect pathogenesis, which might lead in the end to therapeutic failure, could also occur inside multispecies biofilms, in which genetically resistant microorganisms are the susceptible pathogens [75]. As an example, the coexistence of *S. aureus* and *C. albicans* inside biofilms determines the enhancement of *S. aureus* resistance to vancomycin [76]. Therefore, the decrease of microbial adhesion represents one of the main concerns of the current research in the field of biomaterials and medical devices.

In the following, we propose some relative contributions of specific and nonspecific mechanisms in order to explain, to some extent, the efficiency manifested by our fabricated coatings to prevent the microbial adhesion. Therefore, surface features like wetting behavior and material surface characteristics (topography), corroborated with metal ions release can stand as key-factors able to modulate the adhesion of microbes and their subsequent survival on the surface of the synthesized structures.

Water is considered as a major interfacial host in all living environments, and it can affect the capacity of protein adsorption [77] and cellular adhesion [78]. Therefore, to interpret the microbial behavior, this parameter must be carefully taken into consideration. In this respect, one possible mechanism able to explain the antimicrobial activity of synthesized structures is based on their wetting properties and, consequently, on their surface energy values [38]. Therefore, a hydrophilic behavior and high values of surface energy [21] might enhance the overall antimicrobial properties of our fabricated coatings. In addition, the anti-biofilm activity might be explained by repulsive forces which will occur between anionic-coated surfaces (associated with the presence of hydroxyl hydrophilic functional groups) and the *S. aureus*/*C. albicans* biofilms matrix, which is also negatively charged, due to its main component, represented by self-produced exopolysaccharides [38]. Moreover, coatings will facilitate the formation of a highly alkaline medium, consequently leading to the destruction of lipids, which are the main component of microbial cell membrane, followed by microbial cells lysis [79]. When discussing anti-biofilm properties of obtained coatings, one must also consider that the adhesion of microbial cells from aqueous suspensions follows the thermodynamic model. The surface energy of microbial cells is typically smaller than the surface energy of liquids in which cells are suspended, causing cells to attach preferentially to hydrophobic materials (i.e., materials with lower surface energies). Therefore, a hydrophilic behavior, such that of our coatings, and the subsequent

formation of hydration layers could disrupt the initial step of microbial biofilm formation, represented by the adhesion of microbial cells to a surface [80].

Another factor to explain the adhesion of microorganisms is related to the surface characteristics of the material. Therefore, the reduction of microorganisms can be investigated as a function of surface topographic parameters. Among the surface properties, surface roughness and topography have been the most investigated topics in dental biofilm researches. There exists a general perception according to which an increase in surface roughness can promote bacterial colonization due to the increase in contact area between the material surface and bacterial cells, in other words, due to extended surface area available for attachment [81]. Thus, smoothening the surfaces to nanometer-scale roughness was demonstrated to reduce biofilm formation [82]. We note that a roughness (R_a) value of 0.2 μm was reported to be the threshold for maximum reduction of bacterial adhesion on abutment surfaces [83]. In this respect, R_a values inferred in our cases, which are (19–46) times smaller than this threshold, should be emphasized.

Moreover, it was recognized that R_{ku} and R_{sk} are parameters of key-importance when describing surface roughness of calcified tissue implants [84] because osteogenic cells' adhesion is sensitive to the stress concentrations which derive from the presence of sharp heights at the implant-tissue interface [85], likewise they can be considered against bacterial proliferation [86]. Inferred values for skewness and kurtosis parameters indicated a sharper heights (R_{ku} ~5.6) distribution of surface features in case of Li-P structures as compared with Li-0 and Li-C ones (R_{ku} ~3.1 and ~3.5), with more peaks than valleys ($R_{sk} > 0$) and that these peaks and valleys are much closer in height and depth for Li-P coatings (R_{sk} ~0.17) than those of Li-0 and Li-C (R_{sk} of 0.46 and 0.56, respectively). Thus, the average roughness parameter was found to have a similar value (~5 nm) for Li-0 and Li-P coatings, and a double one (~10 nm), for Li-C structures. The positive values of R_{ku} and R_{sk} coefficients could also be related to less available surface-active sites [78,80], and, consequently, could stay at the origin of the inhibition of microbial development on the surface of synthesized structures.

Last but not least, there are reports in the literature on the antibacterial potential of antibiotics/antibacterial substances-loaded HA, but very few refer to antifungal-loaded cement drug delivery [87]. We stress upon that there are even fewer reports dedicated to the antibacterial activity of lithium [88]. It was demonstrated that the antibacterial/anti-biofilm effect can become more evident when extending the exposure to metal [89]. Therefore, one of the proposed mechanisms of action could be the metal accumulation inside bacterial cells, followed by the cellular wall disruption and, eventually, cellular lysis. By extending the proposed mechanism, we can speculate that the amount of lithium ions released from our synthesized materials was enough to accumulate in the microbial cells and to alter the culture media. By affecting their multiplication and phenotypic switching capacity, their further progress is slowed down. These assumptions were confirmed by the results of our study, the lithium-doped samples showing a more pronounced inhibitory effect after 48 and 72 h of incubation, respectively.

5. Conclusions

Simple and lithium-doped biological-derived hydroxyapatite (BHA) coatings were fabricated by Pulsed Laser Deposition onto medical-grade titanium substrates.

In vitro biocompatibility investigations proved that synthesized layers were non-cytotoxic on all tested cell lines, respectively MG-63 osteosarcoma derived cells, human skin new initiated dermal fibroblasts and immortalized keratinocytes, and did not interfere with their cellular cycle phases. In addition, synthesized structures drastically inhibited the ability of *S. aureus* and *C. albicans*, two microorganisms well-known for their complex genetic resistance mechanisms and involvement in the etiology of medical devices-associated biofilm infections, to develop mature biofilms. The anti-fungal biofilm activity has become significant after 12 h of incubation in the case of *C. albicans* and after 24 h for *S. aureus* biofilm, and persisted with high intensity for 72 h. The anti-biofilm activity of obtained coatings could be explained in terms of their surface characteristics, such as

hydrophilic character, associated to a high value of the surface energy, or low values of surface roughness (in the range of 5–10 nm).

We consider that these combined characteristics can be important for the protection of biomedical equipment against contamination by nosocomial infections of any sort, as well as for the long life exploiting of various implants and could therefore offer guidance towards the suitability of lithium-doped BHA structures for future biomedical applications.

Author Contributions: Conceptualization, L.D. and A.P.; Data Curation, M.C.C., G.P.-P., M.A. and A.A.; Investigation, M.C.C., G.P.-P., C.B., G.P.G. and M.A.; Methodology, L.D. and A.P.; Supervision, L.D. and A.P.; Validation, L.D. and A.P.; Writing—Original Draft, L.D.; Writing—Review and Editing, L.D., M.C.C. and A.P.

Funding: This work was supported by a grant of Ministry of Research and Innovation, CNCS-UEFISCDI, No. PN-III-P1-1.1-PD-2016-1568 (PD 6/2018), within PNCDI III. LD, GPP and ACP acknowledge with thanks the partial support of the Romanian National Authority for Scientific Research and Innovation, CNCS-UEFISCDI, under No. PN-II-RU-TE-2014-1570 (TE 108/2015) and Core Programme–Contract 3N/2018. LD and ACP acknowledge the partial support of the Romanian National Authority for Scientific Research and Innovation, CNCS—UEFISCDI, under No. PN-III-P2-2.1-PED-2016-1309 (Contract No. 241/2017).

Acknowledgments: All authors thank F.N Oktar for providing simple biological-derived HA powders and G.E. Stan and V. Craciun for useful discussions.

Conflicts of Interest: The authors declare no conflict of interest.

References

1. Rabin, N.; Zheng, Y.; Opoku-Temeng, C.; Du, Y.; Bonsu, E.; Sintim, H.O. Biofilm formation mechanisms and targets for developing anti-biofilm agents. *Future Med. Chem.* **2015**, *7*, 493–512. [CrossRef] [PubMed]
2. Coughlan, L.M.; Cotter, P.D.; Hill, C.; Alvarez-Ordóñez, A. New weapons to fight old enemies: Novel strategies for the (bio) control of bacterial biofilms in the food industry. *Front. Microbiol.* **2016**, *7*, 400–405. [CrossRef]
3. Del Pozo, J.L. Biofilm-related disease. *Expert Rev. Anti-Infect. Ther.* **2018**, *16*, 51–65. [CrossRef] [PubMed]
4. Petrachi, T.; Resca, E.; Piccinno, M.S.; Biagi, F.; Strusi, V.; Dominici, M.; Veronesi, E. An alternative approach to investigate biofilm in medical devices: A feasibility study. *Int. J. Environ. Res. Public Health* **2017**, *14*, 1587. [CrossRef] [PubMed]
5. Renner, L.D.; Weibel, D.B. Physicochemical regulation of biofilm formation. *MRS Bull.* **2011**, *36*, 347–355. [CrossRef] [PubMed]
6. Claessen, D.; Rozen, D.E.; Kuipers, O.P.; Søgaard-Andersen, L.; Van Wezel, G.P. Bacterial solutions to multicellularity: A tale of biofilms, filaments and fruiting bodies. *Nat. Rev. Microbiol.* **2014**, *12*, 115–124. [CrossRef] [PubMed]
7. Joo, H.-S.; Michael, O. Molecular basis of in-vivo biofilm formation by bacterial pathogens. *Chem. Biol.* **2012**, *19*, 1503–1513. [CrossRef] [PubMed]
8. Lazar, V. Quorum sensing in biofilms—How to destroy the bacterial citadels or their cohesion/power? *Anaerobe* **2011**, *17*, 280–285. [CrossRef] [PubMed]
9. Olar, R.; Badea, M.; Marinescu, D.; Chifiriuc, M.C.; Bleotu, C.; Grecu, M.N.; Iorgulescu, E.E.; Lazar, V. *N*,*N*-dimethylbiguanide complexes displaying low cytotoxicity as potential large spectrum antimicrobial agents. *Eur. J. Med. Chem.* **2010**, *45*, 3027–3034. [CrossRef] [PubMed]
10. Limban, C.; Missir, A.V.; Nuta, D.C.; Caproiu, M.T.; Morusciag, L.; Chirita, C.; Cupii, A.; Gurgu, H. Advances in research of new 2-((4-ethylphenoxy)methyl)-*N*-(arylcarbamothioyl)benzamides. *Farmacia* **2015**, *63*, 376–380.
11. Limban, C.; Missir, A.V.; Nuţă, D.C.; Căproiu, M.T.; Papacocea, M.T.; Chiriţă, C.O. Synthesis of some new 2-((4-chlorophenoxy)methyl)-*N*-(arylcarbamothioyl) benzamides as potential antifungal agents. *Farmacia* **2016**, *64*, 775–779.
12. Boucher, H.W.; Talbot, G.H.; Bradley, J.S. Bad bugs, no drugs: No ESKAPE! An update from the infectious diseases society of America. *Clin. Infect. Dis.* **2009**, *48*, 1–12. [CrossRef] [PubMed]
13. Anghel, I.; Holban, A.M.; Andronescu, E.; Grumezescu, A.M.; Chifiriuc, M.C. Efficient surface functionalization of wound dressings by a phytoactivenanocoating refractory to Candida albicans biofilm development. *Biointerphases* **2013**, *8*, 12. [CrossRef] [PubMed]

14. Chifiriuc, M.C.; Grumezescu, A.M.; Andronescu, E.; Ficai, A.; Cotar, A.I.; Grumezescu, V.; Bezirtzoglou, E.; Lazar, V.; Radulescu, R. Water dispersible magnetite nanoparticles influence the efficacy of antibiotics against planktonic and biofilm embedded enterococcus faecalis cells. *Anaerobe* **2013**, *22*, 14–19. [CrossRef] [PubMed]
15. Dorozhkin, S.V. Calcium orthophosphates: Occurrence properties biomineralization pathological calcification and biomimetic applications. *Biomatter* **2011**, *1*, 121–164. [CrossRef] [PubMed]
16. Graziani, G.; Boi, M.; Bianchi, M. A review on ionic substitutions in hydroxyapatite thin films: Towards complete biomimetism. *Coatings* **2018**, *8*, 269. [CrossRef]
17. Lambert, F.; Angélique, L.; Pierre, D.; Sophie, S.; Pierre, L.; Eric, R. Influence of space-filling materials in subantral bone augmentation: Blood clot vs. autogenous bone chips vs. bovine hydroxyapatite. *Clin. Oral Implant. Res.* **2011**, *22*, 538–545. [CrossRef] [PubMed]
18. Gunduz, O.; Eray, M.E.; Sibel, D.; Serdar, S.; Simeon, A.; Faik, N.O. Composites of bovine hydroxyapatite (BHA) and ZnO. *J. Mater. Sci.* **2008**, *43*, 2536–2540. [CrossRef]
19. Oktar, F.N.; Agathopoulos, S.; Ozyegin, L.S.; Gunduz, O.; Demirkol, N.; Bozkurt, Y.; Salman, S. Mechanical properties of bovine hydroxyapatite (BHA) composites doped with SiO_2, MgO, Al_2O_3, and ZrO_2. *J. Mater. Sci. Mater. Med.* **2007**, *18*, 2137–2143. [CrossRef]
20. Duta, L.; Mihailescu, N.; Popescu, A.C.; Luculescu, C.R.; Mihailescu, I.N.; Cetin, G.; Gunduz, O.; Oktar, F.N.; Popa, A.C.; Kuncser, A.; et al. Comparative physical, chemical and biological assessment of simple and titanium-doped ovine dentine-derived hydroxyapatite coatings fabricated by pulsed laser deposition. *Appl. Surf. Sci.* **2017**, *413*, 129–139. [CrossRef]
21. Popescu, A.C.; Florian, P.E.; Stan, G.E.; Popescu-Pelin, G.; Zgura, I.; Enculescu, M.; Oktar, F.N.; Trusca, R.; Sima, L.E.; Roseanu, A.; et al. Physical-chemical characterization and biological assessment of simple and lithium-doped biological-derived hydroxyapatite thin films for a new generation of metallic implants. *Appl. Surf. Sci.* **2018**, *439*, 724–735. [CrossRef]
22. Duta, L.; Oktar, F.N.; Stan, G.E.; Popescu-Pelin, G.; Serban, N.; Luculescu, C.; Mihailescu, I.N. Novel doped hydroxyapatite thin films obtained by pulsed laser deposition. *Appl. Surf. Sci.* **2013**, *265*, 41–49. [CrossRef]
23. Gunduz, O.; Ahmad, Z.; Ekren, N.; Agathopoulos, S.; Salman, S.; Oktar, F.N. Reinforcing of biologically derived apatite with commercial inert glass. *J. Thermoplast. Compos. Mater.* **2009**, *22*, 407–419. [CrossRef]
24. Khandan, A.; Majid, A.; Neriman, O.; Hamid, G. Study of the bioactivity, wettability and hardness behaviour of the bovine hydroxyapatite-diopside bio-nanocomposite coating. *J. Taiwan Inst. Chem. Eng.* **2016**, *60*, 538–546. [CrossRef]
25. Mihailescu, N.; Stan, G.E.; Duta, L.; Mariana, C.C.; Coralia, B.; Sopronyi, M.; Luculescu, C.; Oktar, F.N.; Mihailescu, I.N. Structural, compositional, mechanical characterization and biological assessment of bovine-derived hydroxyapatite coatings reinforced with MgF_2 or MgO for implants functionalization. *Mater. Sci. Eng. C* **2016**, *59*, 863–874. [CrossRef] [PubMed]
26. Gunduz, O.; Godec, C.; Ahmad, Z.; Gokce, H.; Yetmez, M.; Kalkandelen, C.; Sahin, Y.M.; Oktar, F.N. Preparation and evaluation of cerium oxide-bovine hydroxyapatite composites for biomedical engineering applications. *J. Mech. Behav. Biomed.* **2014**, *35*, 70–76. [CrossRef] [PubMed]
27. Boutinguiza, M.; Pou, J.; Comesaña, R.; Lusquiños, F.; de Carlos, A.; León, B. Biological hydroxyapatite obtained from fish bones. *Mater. Sci. Eng. C* **2012**, *32*, 478–486. [CrossRef]
28. Eisenhart, S. *EU Regulation 722. New EU Animal Tissue Regulations in Effect for Some Medical Devices*; Emergo: Hong Kong, China, 2013; Available online: https://www.emergobyul.com/blog/2013/09/new-eu-animal-tissue-regulations-effect-some-medical-devices (accessed on 16 January 2019).
29. *ISO 22442-1 Medical Devices Utilizing Animal Tissues and Their Derivatives—Part 1: Application of Risk Management*; International Organization for Standardization: Berlin, Germany, 2015.
30. Eaton, P.; West, P. *Atomic Force Microscopy*, 1st ed.; Oxford University Press: Oxford, UK, 2010; pp. 1–256.
31. Boukamp, P.; Petrussevska, R.T.; Breitkreutz, D.; Hornung, J.; Markham, A.; Fusenig, N.E. Normal keratinization in a spontaneously immortalized aneuploid human keratinocyte cell line. *J. Cell Biol.* **1988**, *106*, 761–771. [CrossRef]
32. *ISO 10993-5 Biological Evaluation of Medical Devices—Part 5: Tests for In Vitro Cytotoxicity*; International Organization for Standardization: Berlin, Germany, 2009.

33. Duta, L.; Ristoscu, C.; Stan, G.E.; Husanu, M.A.; Besleaga, C.; Chifiriuc, M.C.; Lazar, V.; Bleotu, C.; Miculescu, F.; Mihailescu, N.; et al. New bio-active, antimicrobial and adherent coatings of nanostructured carbon double-reinforced with silver and silicon by Matrix-Assisted Pulsed Laser Evaporation for medical applications. *Appl. Surf. Sci.* **2018**, *441*, 871–883. [CrossRef]
34. Stan, G.E.; Popescu, A.C.; Mihailescu, I.N.; Marcov, D.A.; Mustata, R.C.; Sima, L.E.; Petrescu, S.M.; Ianculescu, A.; Trusca, R.; Morosanu, C.O. On the bioactivity of adherent Bioglass thin films synthesized by magnetron sputtering techniques. *Thin Solid Films* **2010**, *518*, 5955–5964. [CrossRef]
35. Clover, J.; Gowen, M. Are MG-63 and HOS TE85 human osteosarcoma cell lines representative models of the osteoblastic phenotype? *Bone* **1994**, *15*, 585–591. [CrossRef]
36. Skindersoe, M.E.; Krogfelt, K.A.; Blom, A.; Jiang, G.; Prestwich, G.D.; Mansell, J.P. Dual action of lysophosphatidate-functionalised titanium: Interactions with human (MG63) Osteoblasts and methicillin resistant staphylococcus aureus. *PLoS ONE* **2015**, *10*, e0143509. [CrossRef] [PubMed]
37. Mitik-Dineva, N.; Wang, J.; Truong, V.K.; Stoddart, P.; Malherbe, F.; Crawford, R.J.; Ivanova, E.P. *Escherichia coli*, pseudomonas aeruginosa, and staphylococcus aureus attachment patterns on glass surfaces with nanoscale roughness. *Curr. Microbiol.* **2009**, *58*, 268–273.
38. Chua, P.-H.; Neoh, K.-G.; Kang, E.-T.; Wang, W. Surface functionalization of titanium with hyaluronic acid/chitosan polyelectrolyte multilayers and RGD for promoting osteoblast functions and inhibiting bacterial adhesion. *Biomaterials* **2008**, *29*, 1412–1421. [CrossRef] [PubMed]
39. Paulone, S.; Ardizzoni, A.; Tavanti, A.; Piccinelli, S.; Rizzato, C.; Lupetti, A.; Colombari, B.; Pericolini, E.; Polonelli, L.; Magliani, W.; et al. The synthetic killer peptide KP impairs Candida albicans biofilm in vitro. *PLoS ONE* **2017**, *13*, e0181278. [CrossRef] [PubMed]
40. Tsui, C.; Kong, E.F.; Jabra-Rizk, M.A. Pathogenesis of Candida albicans biofilm. *Pathog. Dis.* **2016**, *74*, ftw018. [CrossRef] [PubMed]
41. Groza, A.; Ciobanu, C.S.; Popa, C.L.; Iconaru, S.L.; Chapon, P.; Luculescu, C.; Ganciu, M.; Predoi, D. Structural properties and antifungal activity against Candida albicans biofilm of different composite layers based on Ag/Zn doped Hydroxyapatite-polydimethylsiloxanes. *Polymers* **2016**, *8*, 131. [CrossRef]
42. Tite, T.; Popa, A.C.; Balescu, L.M.; Bogdan, I.M.; Pasuk, I.; Ferreira, J.M.F.; Stan, G.E. Cationic substitutions in hydroxyapatite: Current status of the derived biofunctional effects and their in vitro interrogation methods. *Materials* **2018**, *11*, 2081. [CrossRef]
43. Cleare, A.; Pariante, C.M.; Young, A.H.; Anderson, I.M.; Christmas, D.; Cowen, P.J.; Dickens, C.; Ferrier, I.N.; Geddes, J.; Gilbody, S.; et al. Evidence-based guidelines for treating depressive disorders with antidepressants: A revision of the 2008 British Association for Psychopharmacology guidelines. *J. Psychopharmacol.* **2015**, *29*, 459–525. [CrossRef]
44. Cohen, O.; Rais, T.; Lepkifker, E.; Vered, I. Lithium carbonate therapy is not a risk factor for osteoporosis. *Horm. Metab. Res.* **1998**, *30*, 594–597. [CrossRef]
45. Nordenstrom, J.; Elvius, M.; Bagedahl-Strindlund, M.; Zhao, B.; Torring, O. Biochemical hyperparathyroidism and bone-mineral status in patients treated long-term with lithium. *Metabolism* **1994**, *43*, 1563–1567. [CrossRef]
46. Satija, N.K.; Sharma, D.; Afrin, F.; Tripathi, R.P.; Gangenahalli, G. High throughput transcriptome profiling of lithium stimulated human mesenchymal stem cells reveals priming towards osteoblastic lineage. *PLoS ONE* **2013**, *8*, e55769. [CrossRef] [PubMed]
47. Zamani, A.; Omrani, G.R.; Nasab, M.M. Lithium's effect on bone mineral density. *Bone* **2009**, *44*, 331–334. [CrossRef]
48. Yang, M.L.; Li, J.J.; So, K.F.; Chen, J.Y.H.; Cheng, W.S.; Wu, J.; Wang, Z.M.; Gao, F.; Young, W. Efficacy and safety of lithium carbonate treatment of chronic spinal cord injuries: A double-blind, randomized, placebo-controlled clinical trial. *Spinal Cord* **2012**, *50*, 141–146. [CrossRef] [PubMed]
49. Gitlin, M. Lithium side effects and toxicity: Prevalence and management strategies. *Int. J. Bipolar Disord.* **2016**, *4*, 27. [CrossRef] [PubMed]
50. Ott, M.; Stegmayr, B.; Salander, R.E.; Werneke, U. Lithium intoxication: Incidence, clinical course and renal function—A population-based retrospective cohort study. *J. Psychopharmacol.* **2016**, *30*, 1008–1019. [CrossRef]
51. Rybakowski, J.K. Challenging the negative perception of lithium and optimizing its long-term administration. *Front. Mol. Neurosci.* **2018**, *11*, 349. [CrossRef]

52. Post, R.M. The new news about lithium: An underutilized treatment in the United States. *Neuropsychopharmacology* **2018**, *43*, 1174–1179. [CrossRef]
53. Mayer, I.; Berger, U.; Markitziu, A.; Gidalia, I. The uptake of lithium ions by synthetic carbonated hydroxyapatite. *Calcif. Tissue Int.* **1986**, *38*, 293–295. [CrossRef]
54. Koutsoukos, P.G.; Nancollas, G.H. The effect of lithium on the precipitation of hydroxyapatite from aqueous solutions. *Colloids Surf.* **1986**, *17*, 361–370. [CrossRef]
55. Shainberg, A.P.M.; Valério, P.; Zonari, A.; Oktar, F.N.; Ozyegin, L.S.; Graça, M.P.F.; Leite, M.F.; Goes, A.M. Attachment and proliferation of osteoblasts on lithium-hydroxyapatite composites. *Adv. Mater. Sci. Eng.* **2012**, *2012*, 650574. [CrossRef]
56. Gough, J.; Notingher, I.; Hench, L.L. Osteoblast attachment and mineralized nodule formation on rough and smooth 45S5 bioactive glass monoliths. *J. Biomed. Mater. Res. Part A* **2004**, *68*, 640–650. [CrossRef] [PubMed]
57. Wang, Y.; Yang, X.; Gu, Z.; Qin, H.; Li, L.; Liu, J.; Yu, X. In vitro study on the degradation of lithium-doped hydroxyapatite for bone tissue engineering scaffold. *Mater. Sci. Eng. C* **2016**, *66*, 185–192. [CrossRef] [PubMed]
58. Meunier, P.J.; Roux, C.; Seeman, E.; Ortolani, S.; Badurski, J.E.; Spector, T.D.; Cannata, J.; Balogh, A.; Lemmel, E.M.; Pors-Nielsen, S.; et al. The effects of strontium ranelate on the risk of vertebral fracture in women with postmenopausal osteoporosis. *N. Engl. J. Med.* **2004**, *350*, 459–468. [CrossRef] [PubMed]
59. Wexler, E.M.; Geschwind, D.H.; Palmer, T.D. Lithium regulates adult hippocampal progenitor development through canonical Wnt pathway activation. *Mol. Psychiatry* **2008**, *13*, 285–292. [CrossRef] [PubMed]
60. Khorami, M.; Hesaraki, S.; Behnamghader, A.; Nazarian, H.; Shahrabi, S. In vitro bioactivity and biocompatibility of lithium substituted 45S5 bioglass. *Mater. Sci. Eng. C* **2011**, *31*, 1584–1592. [CrossRef]
61. Liu, F.; Zhang, X.; Yu, X.; Xu, Y.; Feng, T.; Ren, D. In vitro study in stimulating the secretion of angiogenic growth factors of strontium-doped calcium polyphosphate for bone tissue engineering. *J. Mater. Sci. Mater. Med.* **2011**, *22*, 683–692. [CrossRef]
62. Tang, G.; Xu, J.; Chen, R.; Qian, Y.; Shen, G. Lithium delivery enhances bone growth during midpalatal expansion. *J. Dent. Res.* **2011**, *90*, 336–340. [CrossRef]
63. Oh, S.H.; Choi, S.Y.; Choi, S.H.; Lee, Y.K.; Kim, K.N. The influence of lithium fluoride on in vitro biocompatibility and bioactivity of calcium aluminate-PMMA composite cement. *J. Mater. Sci. Mater. Med.* **2004**, *15*, 25–33. [CrossRef]
64. Miguez-Pacheco, V.; Büttner, T.; Maçon, A.L.B.; Jones, J.R.; Fey, T.; de Ligny, D.; Greil, P.; Chevalier, J.; Malchere, A.; Boccaccini, A.R. Development and characterization of lithium-releasing silicate bioactive glasses and their scaffolds for bone repair. *J. Non-Cryst. Solids* **2016**, *432*, 65–72. [CrossRef]
65. Keong, L.C.; Halim, A.S. In vitro models in biocompatibility assessment for biomedical-grade chitosan derivatives in wound management. *Int. J. Mol. Sci.* **2009**, *10*, 1300–1313. [CrossRef] [PubMed]
66. Buskermolen, J.K.; Reijnders, C.M.A.; Spiekstra, S.W.; Steinberg, T.; Kleverlaan, C.J.; Feilzer, A.J.; Bakker, A.D.; Gibbs, S. Development of a full-thickness human gingiva equivalent constructed from immortalized keratinocytes and fibroblasts. *Tissue Eng. Part C Methods* **2016**, *22*, 781–791. [CrossRef] [PubMed]
67. Schalock, P.C.; Crawford, G.; Nedorost, S.; Scheinman, P.L.; Atwater, A.R.; Mowad, C.; Brod, B.; Ehrlich, A.; Watsky, K.L.; Sasseville, D.; et al. Patch testing for evaluation of hypersensitivity to implanted metal devices: A perspective from the american contact dermatitis society. *Dermatitis* **2016**, *27*, 241–247. [CrossRef] [PubMed]
68. An, Y.H.; Friedman, R.J. Concise review of mechanisms of bacterial adhesion to biomaterial surfaces. *J. Biomed. Mater. Res. (Appl. Biomater.)* **1998**, *43*, 338–348. [CrossRef]
69. Lieb, J. Lithium and antidepressants: Inhibiting eicosanoids, stimulating immunity, and defeating microorganisms. *Med. Hypotheses* **2002**, *59*, 429–432. [CrossRef]
70. Fabrizi, C.; Pompili, E.; Somma, F.; De Vito, S.; Ciraci, V.; Artico, M.; Lenzi, P.; Fornai, F.; Fumagalli, L. Lithium limits trimethyltin-induced cytotoxicity and proinflammatory response in microglia without affecting the concurrent autophagy impairment. *J. Appl. Toxicol.* **2017**, *37*, 207–213. [CrossRef]
71. Moghanian, A.; Firoozi, S.; Tahriri, M.; Sedghi, A. A comparative study on the in vitro formation of hydroxyapatite, cytotoxicity and antibacterial activity of 58S bioactive glass substituted by Li and Sr. *Mater. Sci. Eng. C Mater. Biol. Appl.* **2018**, *91*, 349–360. [CrossRef]
72. Douglas, L.J. Candida biofilms and their role in infection. *Trends Microbiol.* **2003**, *11*, 30–36. [CrossRef]

73. Sadik, O.; Gheorghe, I.; Chifiriuc, M.C. Virulence and pathogenicity aspects in Candida albicans infections. *Rev. Biol. Biomed. Sci.* **2018**, *1*, 11–16. [CrossRef]
74. Kart, D.; Tavernier, S.; Van Acker, H.; Nelis, H.J.; Coenye, T. Activity of disinfectants against multispecies biofilms formed by Staphylococcus aureus. Candida albicans and Pseudomonas aeruginosa. *Biofouling* **2014**, *30*, 377–383. [CrossRef]
75. Jenkinson, H.F.; Lamont, R.J. Oral microbial communities in sickness and in health. *Trend. Microbiol.* **2005**, *13*, 589–595. [CrossRef] [PubMed]
76. Harriott, M.M.; Noverr, M.C. Candida albicans and Staphylococcus aureus form polymicrobial biofilms: Effects on antimicrobial resistance. *Antimicrob. Agents Chemother.* **2009**, *53*, 3914–3922. [CrossRef] [PubMed]
77. D'Elia, N.L.; Gravina, N.; Ruso, J.M.; Marco-Brown, J.L.; Sieben, J.M.; Messina, P.V. Albumin-mediated deposition of bone-like apatite onto nano-sized surfaces: Effect of surface reactivity and interfacial hydration. *J. Colloid Interface Sci.* **2017**, *494*, 345–354. [CrossRef] [PubMed]
78. Giraldez, M.J.; Resua, C.G.; Lira, M.; Oliveira, M.E.C.R.; Magariños, B.; Toranzo, A.E.; Yebra-Pimentel, E. Contact lens hydrophobicity and roughness effects on bacterial adhesion. *Optom. Vis. Sci.* **2010**, *87*, E426–E431. [CrossRef]
79. Tamburic, S.D.; Vuleta, G.M.; Ognjanovic, J.M. In vitro release of calcium and hydroxyl ions from two types of calcium hydroxide preparations. *Int. Endod. J.* **1993**, *26*, 125–130. [CrossRef]
80. Absolom, D.R.; Lamberti, F.V.; Policova, Z.; Zingg, W.; van Oss, C.J.; Neumann, A.W. Surface thermodynamics of bacterial adhesion. *Appl. Environ. Microb.* **1983**, *46*, 90–97.
81. Anselme, K.; Davidson, P.; Popa, A.; Giazzon, M.; Liley, M.; Ploux, L. The interaction of cells and bacteria with surfaces structured at the nanometre scale. *Acta Biomater.* **2010**, *6*, 3824–3846. [CrossRef]
82. Ionescu, A.; Wutscher, E.; Brambilla, E.; Schneider-Feyrer, S.; Giessibl, F.J.; Hahnel, S. Influence of surface properties of resin-based composites on in vitro streptococcus mutans biofilm development. *Eur. J. Oral Sci.* **2012**, *120*, 458–465. [CrossRef]
83. Quirynen, M.; Bollen, C.M.; Papaioannou, W.; Van Eldere, J.; van Steenberghe, D. The influence of titanium abutment surface roughness on plaque accumulation and gingivitis: Short-term observations. *Int. J. Oral Maxillofac. Implant.* **1996**, *11*, 169–178.
84. Hansson, K.N.; Hansson, S. Skewness and kurtosis: Important parameters in the characterization of dental implant surface roughness—A computer simulation. *ISRN Mater. Sci.* **2011**, *2011*, 305312. [CrossRef]
85. Cheng, T.; Chen, Y.; Nie, X. Insertion torques influenced by bone density and surface roughness of HA–TiO_2 coatings. *Thin Solid Films* **2013**, *549*, 123–130. [CrossRef]
86. Han, L.; Wang, M.; Sun, H.; Li, P.; Wang, K.; Ren, F.; Lu, X. Porous titanium scaffolds with self-assembled micro/nano hierarchical structure for dual functions of bone regeneration and anti-infection. *J. Biomed. Mater. Res. A* **2017**, *105*, 3482–3492. [CrossRef] [PubMed]
87. Karr, J.C.; Lauretta, J. In vitro activity of calcium sulfate and hydroxyapatite antifungal disks loaded with amphotericin B or voriconazole in consideration for adjunctive osteomyelitis management. *J. Am. Podiatr. Med. Assoc.* **2015**, *105*, 104–110. [CrossRef] [PubMed]
88. Khalid, A.Q.; AlJohny, B.O.; Wainwright, M. Antibacterial effects of pure metals on clinically important bacteria growing in planktonic cultures and biofilms. *Afr. J. Microbiol. Res.* **2014**, *8*, 1080–1088.
89. Harrison, J.C.; Zyla, T.R.; Bardes, E.S.; Lew, D.J. Stress-specific activation mechanisms for the "cell integrity" MAPK pathway. *J. Biol. Chem.* **2004**, *279*, 2616–2622.